Feasibility of an acoustic liner applied to a Fenestron: experimentation

Victor Lafont, Delphine Sebbane, Frank Simon, Jean-Paul Pinacho, Julien Caillet

▶ **To cite this version:**

Victor Lafont, Delphine Sebbane, Frank Simon, Jean-Paul Pinacho, Julien Caillet. Feasibility of an acoustic liner applied to a Fenestron: experimentation. Internoise 2024, Aug 2024, Nantes, France. ⟨hal-04778483⟩

HAL Id: hal-04778483

https://hal.science/hal-04778483v1

Submitted on 13 Nov 2024

HAL is a multi-disciplinary open access archive for the deposit and dissemination of scientific research documents, whether they are published or not. The documents may come from teaching and research institutions in France or abroad, or from public or private research centers.

L'archive ouverte pluridisciplinaire **HAL**, est destinée au dépôt et à la diffusion de documents scientifiques de niveau recherche, publiés ou non, émanant des établissements d'enseignement et de recherche français ou étrangers, des laboratoires publics ou privés.

HAL Authorization

FEASIBILITY OF AN ACOUSTIC LINER APPLIED TO A FENESTRON™

Victor Lafont, Delphine Sebbane, Frank Simon, Elia Pautard
DMPE, ONERA, Université de Toulouse,
31000 Toulouse, France

Julien Caillet, Jean-Paul Pinacho
Airbus Helicopters, Aéroport International Marseille-Provence,
13725 Marignane Cedex

ABSTRACT

A helicopter anti-torque system significantly contributes to radiated noise. The Fenestron™ anti-torque system used on Airbus helicopters, reduces this noise through masking effects and blade distribution modulation. This paper explores integrating acoustic treatments into the Fenestron™, similar to those used in aircraft engine nacelles, to further decrease the anti-torque system noise. Numerical simulations are performed to identify the optimal acoustic impedance for these liners, followed by proposing and assessing several liner designs on small-scale experimental benches. Finally, a larger-scale, more representative measurement campaign on a Fenestron™ mock-up with integrated liners demonstrates that a likely significant noise reduction can be attained.

1. NOTATION

Symbols :

α	Acoustic absorption coefficient
ζ	Specific acoustic impedance
f	Frequency, Hz
c_0	Speed of sound in air, m/s
ρ_0	Air density, kg/m^3

Acronyms :

BPF	Blade Passing Frequency
DDOF	Double-Degree of Freedom
LEONAR	Long Elastic Open Neck Acoustic Resonator
RPM	Rotation per Minute
SDOF	Single-Degree of Freedom
SPL	Sound Pressure Level

Copyright Statement
The authors confirm that they, and/or their company or organization, hold copyright on all of the original material included in this paper. The authors also confirm that they have obtained permission, from the copyright holder of any third-party material included in this paper, to publish it as part of their paper. The authors confirm that they give permission, or have obtained permission from the copyright holder of this paper, for the publication and distribution of this paper as part of the ERF proceedings or as individual offprints from the proceedings and for inclusion in a freely accessible web-based repository.

2. INTRODUCTION

Helicopters frequently operate in sensitive areas such as dense urban environments. To decrease the noise levels of their products, helicopter manufacturers develop improved low-noise solutions. The present study focuses on collaborative efforts between ONERA and Airbus Helicopters to reduce the noise emitted by a ducted tail rotor, known as the Fenestron™.

Although the Fenestron™ already offers a noise reduction advantage over conventional anti-torque systems, it remains a significant contributor to the total noise produced by helicopters in climb and hover conditions due to high thrust requirements, or even in cruise conditions. The Fenestron™'s benefits stem from the masking effect of the duct fairing, particularly efficient under track, its relatively low tip speeds, and its modular blade distribution. To further enhance helicopter acceptability, a promising technological solution consists in including acoustic liners into the Fenestron™ design, absorbing sound radiation before it escapes the shroud [1, 2].

Conventional acoustic liners, commonly used in aircraft nacelles, are typically composed of an honeycomb structure topped with a thin perforated plate, forming an array of Helmholtz resonators – this basic assembly is referred to as a single-degree of freedom (SDOF) liner.

The driving parameter for the noise damping power of liners is their specific acoustic impedance, that is the ratio between acoustic pressure p and normal acoustic velocity v_n taken on the facesheet, normalized by the impedance of air $\rho_0 c_0$:

$$\zeta(\omega) = \frac{p}{\rho_0 c_0 v_n} = r(\omega) + j\chi(\omega), \quad (1)$$

where r and χ are respectively called the resistance and the reactance of the liner.

Designing an efficient liner involves accurately tuning the geometries of the perforated plate and of the cavities to match the desired noise damping or acoustic impedance [3]. A complex optimization process using numerical and experimental tools might then be needed, especially when using unconventional geometries [4–8]. ONERA developed a software platform called OPAL (OPtimization of Acoustic Liners) [9, 10] to facilitate this process on various liner geometries, taking into account the surrounding physical environment.

The aim of this study is to numerically design optimal acoustic liners that efficiently reduce the noise within provided constraints (thickness, weight,...) relative to the Fenestron™, and to assess their performance experimentally, both on reduced-scale test rigs and on a full 1/3-scale Fenestron™ mock-up.

Section 3 presents the preliminary numerical simulations used to determine the properties required for the liners. Section 4 then describes the design process for the proposed acoustic liners and the experimental validation of their acoustic behavior on small-scale test benches. Finally, Sections 5 and 6 detail the large-scale campaign conducted on the Fenestron™ mock-up.

3. PRELIMINARY ACOUSTIC MODELIZATION

This section describes the preliminary numerical study that was conducted in order to determine the optimal properties for the integrated liner.

Fenestron™noise obviously depends on flight conditions, such as helicopter weight, flight speed, that correspond to different thrust settings and airflows distributions. In this project, typical settings in relevant flight conditions have been provided by Airbus Helicopters for both the mock-up scale and actual Fenestron™ scale. In general, cruise operations would be performed at low Fenestron™ pitch (and corresponding thrust), while climb conditions at high rate of climb (such as take-off noise certification condition) would be performed at high pitch. On the mock-up, both the RPM and pitch can be controlled, while for actual helicopter operations, RPM would remain almost constant. In this study, the RPM variation capability is used to assess the performance of acoustic liners for a wide range of frequency corresponding to a Fenestron™ tonal content on actual helicopters.

3.1 Fenestron™ model

To assess the Fenestron™ duct effect on acoustic radiation, this study uses a simplified propeller noise formulation implemented in an acoustic finite element model (FEM). The formulation captures steady loading and thickness noise emitted from an isolated propeller, without accounting for changes in flow characteristics or loading conditions due to the duct : these parameters are directly inputs to the model.

3.1.1 Equivalent sources

The near-field pressure is described as a function of rotor thrust and torque using the Garrick and Watkins formulation [11]. This involves concentrating thrust T and torque Q on an annular ring rather than distributing them across the propeller disk, placing the annular ring at an effective propeller radius r_e. Equivalent loading sources on the top and bottom surfaces of the annular ring are then defined (Fig. 1).

The source pressure on the propeller disk (called thickness noise) is defined using Hanson's formulation [12,13]. Equivalent sources are defined on the propeller disk's top and bottom surfaces to capture this thickness noise (Fig. 2).

Each noise source is modeled separately; the resulting pressure fields are combined to determine the total pressure field, propagated across a large acoustic domain terminated by a perfectly matched layer to approximate free-field conditions. The model is solved in the frequency domain at the propeller's 1st blade passing frequency (BPF).

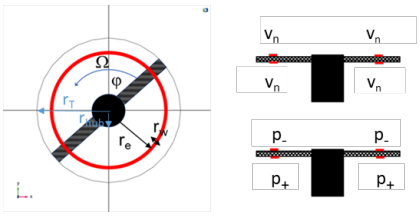

FIGURE 1 – Top view of the effective ring in red (left) and equivalent source distribution for thrust and torque components on a cross section of the propeller disk (right).

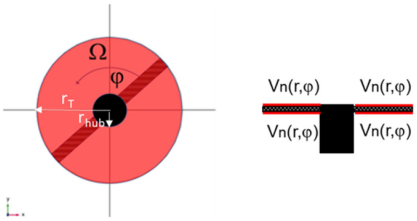

FIGURE 2 – Top view of the propeller disk (left) and equivalent source distribution for thickness noise on a cross section of the propeller disk (right).

3.1.2 Full Fenestron™ model

The first step in defining the full model involves setting up the acoustic model of the internal parts of the 1/3-scale Fenestron™ mock-up, excluding the rotor blades : collector, diffuser, rotor hub, gearbox, shaft fairing, and stator blades (Fig. 3). This model is then imported into COMSOL Multiphysics® to configure it for the mock-up rotor (8 blades, non-modulated distribution).

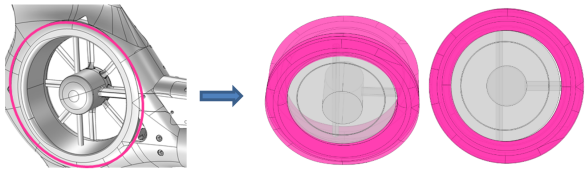

FIGURE 3 – Generation of the COMSOL Multiphysics® model for the internal parts of the 1/3-scale Fenestron™ mock-up.

The second step is to define the area where to compute the radiated acoustic pressure and power (Fig. 4) :

— an hemisphere centered on the rotor and directed towards the ground,
— a flat surface of 2×2 m^2 at 1 m under the center to be able to estimate the acoustic power radiated on a flat surface of 300×300 m^2 at 150 m from the center (under the hypothesis of an identical solid angle).

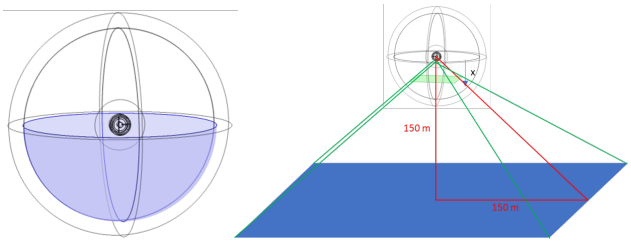

FIGURE 4 – Hemisphere (left) and flat surface (right) to compute the acoustic pressure and power.

3.2 Acoustic liner efficiency

The goal of acoustic treatment is to reduce the radiated acoustic power compared to a rigid diffuser surface. The acoustic treatment is assumed to have a localized reaction, allowing its acoustic response to be simulated using a surface impedance ζ, defined as in Equation 1.

Figure 5 shows the reduction in acoustic power radiated in a configuration with a treated diffuser of impedance ζ, for three values of the reactance χ, compared to the rigid diffuser case. A resistance around 0.5 clearly results in greater reduction than a resistance near 1 (where the absorption coefficient α equals 1 at normal incidence), but the attenuation obtained is more frequency-dependent in that case. A value near 1 provides a more constant attenuation over the considered frequency range.

Tables 1 and 2 below indicate the total noise attenuations (thrust noise, torque, and thickness) for various values of ζ in a configuration with treated diffuser, at 5500 and 11910 RPM. Again, the overall attenuation is greater for low to medium resistances (r<0.5) but it is observed that at such values of r, a small variation on the reactance value (with r fixed) can reduce significantly the noise mitigation, while values of r around 1 provide very stable behaviors when χ varies from -1.5 to 1.5 at fixed resistance.

r \ χ	**-1.5**	**-1**	**-0.5**	**0**	**0.5**	**1**	**1.5**
0.25	1.0	0.2	-2.6	-3.5	-2.5	-1.9	-1.5
0.5	0.3	-0.7	-2.4	-3.0	-2.4	-1.9	-1.5
0.75	-0.2	-1.0	-2.1	-2.5	-2.3	-1.9	-1.5
1	-0.4	-1.1	-1.8	-2.2	-2.1	-1.8	-1.5
1.25	-0.6	-1.1	-1.6	-1.9	-1.9	-1.7	-1.4
1.5	-0.7	-1.1	-1.5	-1.7	-1.7	-1.6	-1.4
1.75	-0.7	-1.0	-1.3	-1.5	-1.5	-1.4	-1.3
2	-0.7	-1.0	-1.2	-1.4	-1.4	-1.4	-1.3

TABLE 1 – Total attenuation (dB). RPM=5500

r \ χ	**-1.5**	**-1**	**-0.5**	**0**	**0.5**	**1**	**1.5**
0.25	-2.8	-3.8	-4.3	-3.3	-1.8	-0.9	-0.5
0.5	-3.3	-4.0	-4.3	-3.5	-2.3	-1.4	-0.9
0.75	-3.3	-3.9	-4.1	-3.5	-2.5	-1.7	-1.2
1	-3.3	-3.7	-3.8	-3.3	-2.6	-1.9	-1.4
1.25	-3.2	-3.5	-3.5	-3.2	-2.6	-2.0	-1.6
1.5	-3.1	-3.3	-3.3	-3.0	-2.6	-2.1	-1.7
1.75	-2.9	-3.1	-3.1	-2.9	-2.5	-2.1	-1.7
2	-2.8	-2.9	-2.9	-2.7	-2.4	-2.1	-1.8

TABLE 2 – Total attenuation (dB). RPM=11900

The value $r = 0.5$ therefore appears to be a good target ; however, since the attenuation obtained in that case depends both of the frequency and of the reactance values, and is therefore highly dependent of the manufacturing uncertainties, aiming for a resistance around 1 is more reliable to ensure good absorption.

Figure 6 shows the pressure fields at 5500 RPM provided by the Fenestron™ rotor without and with treated diffuser and/or collector for a specific impedance $\zeta = 1$. It appears that the collector has an asymmetrical effect with reduction upstream, while the diffuser mainly acts downstream, but that combining the two treatments improves spatial mitigation with a power reduction of 2.9 dB compared to 1.8 dB for the diffuser alone.

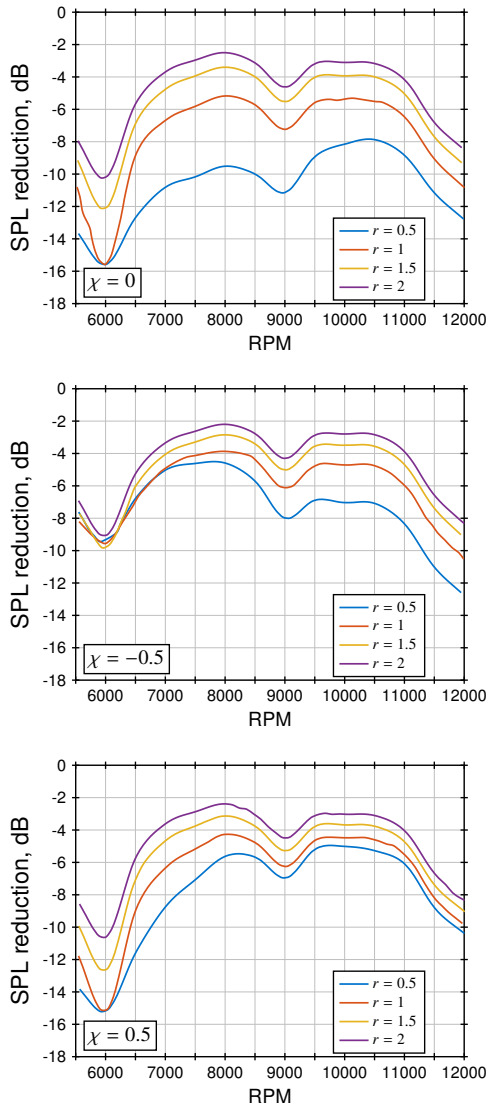

FIGURE 5 – Reduction in acoustic power (dB) provided for torque type noise as a function of the resistance r, at three values of the reactance χ (-0.5, 0 and 0.5).

4. LINER DESIGN

This section presents the optimization that was performed to propose satisfying liner designs, using the OPAL software with the FEM results as a base. The objective is to design a liner able to be implemented in the Fenestron™ diffuser with a reactance close to 0 and a resistance close to 1 in a large frequency range, in order to cover the 1st and 2nd BPFs for a wide range of revolution speeds (RPM from 5500 to 11900).

4.1 OPAL platform

The OPAL software developed by ONERA [9, 10] allows to assemble a large panel of parallel/serial elementary acoustic layers to form a full acoustic liner. The four available elementary acoustic materials are the following :

— porous material (e.g. foam, wiremesh, fabric),
— perforated plate,
— honeycomb cavity,
— LEONAR cell [6].

Each of these elements is modelled according to the equivalent fluid model, with the appropriate end corrections for the perforated plate. The LEONAR cell is an assembly of a perforated plate and a cavity with additional constraints to accurately represent its physical behavior. Any combination of these 4 elements, using the transfer matrix formalism, forms a complete acoustic liner. The physical properties of the liner can then be computed for a given physical environment (flow, temperature, frequency range, duct geometry, liner dimensions) and optimized relatively to weighted objectives such as impedance target, maximum absorption coefficient or transmission loss.

4.2 Optimization process

In this study, several different liner designs [14] whose properties were optimized using OPAL were initially proposed.

The dimensional constraints for the optimized designs are mainly based on industrial concerns :

— maximum total thickness = 42 mm
— minimal thickness of the external layer = 1 mm
— minimal hole diameter = 1 mm

Following the preliminary numerical simulation results, the optimization was conducted with an impedance target $\zeta = 1$, and an incident SPL set to 140 dB (the preliminary numerical simulation with COMSOL Multiphysics® showed that this value is representative of the SPL on the diffuser's surface).

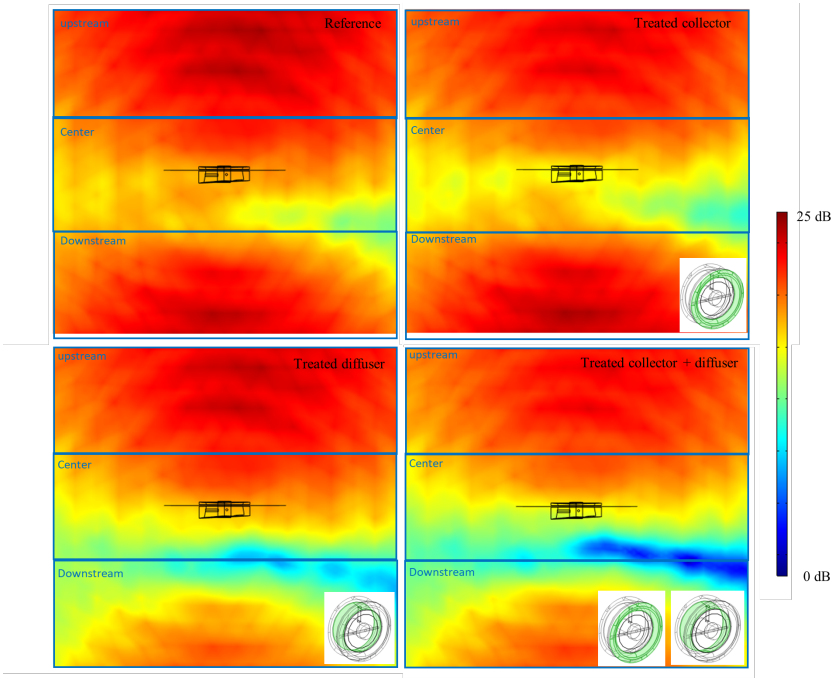

	SPL mitigation, dB			
	Upstream	**Center**	**Downstream**	**Total**
Treated diffuser	-0.7	-1.1	-6	-1.8
Treated collector	-1.3	-1.8	0.6	-0.7
Both	-1.9	-3	-5.1	-2.9

FIGURE 6 – Computed acoustic pressure fields (relative scale dB) and mean SPL mitigation (dB) on the measurement surface for a rotor with fully rigid fairing (reference) and with treated diffuser and/or collector. $\zeta = 1$, RPM = 5500.

4.3 Final designs

Table 3 summarizes the characteristics of the 4 liner candidates. Designs #1 and #2 are conventional perforated liners, while designs #3 and #4 are more complex architectures including LEONAR cells. A basic schematics of each design is shown in Figure 7.

The acoustic absorption coefficients (noted α) of each liner, computed with a (normal) incident SPL of 140 dB, are plotted in Figure 8. The classic SDOF and DDOF designs (#1 and #2) perform quite good near their optimum but are not very absorbent in the lower frequency range ; moreover, the classic DDOF design adds manufacturing complexity but does not seem to provide significantly better absorption than the classic SDOF design. The added value of the more complex designs including LEONAR cells is clear, as liners #3 and #4 show an increased absorption in the lower frequency range and a more broadband behavior.

Impedance tube measurements on small-scale 3D-printed samples were performed to assess the validity of the numerical optimization : results from

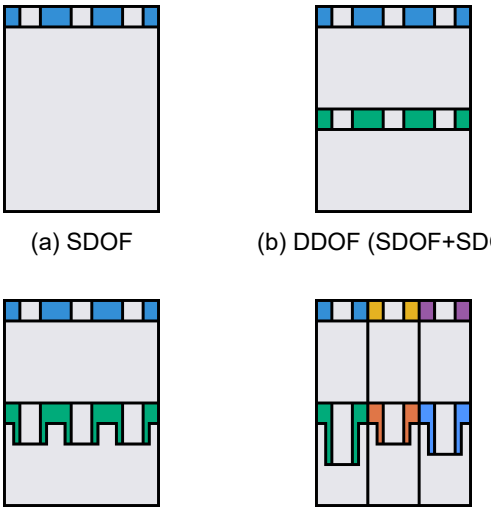

(a) SDOF (b) DDOF (SDOF+SDOF)

(c) DDOF (SDOF+LEO) (d) Metasurface

FIGURE 7 – Schematics of the 4 liner designs (not to scale, proportions not kept)

these measurements are shown in Figure 9 (more details on this experimental validation can be found in [15]). All samples appear to absorb as expected except the conventional DDOF design, which exhibits lower absorption over the whole frequency range. Since it does not provide an advantage over the classic SDOF and appears less effective than all the other designs, it is abandoned. The metasurface design is deemed too complex to be properly integrated into the final mock-up despite its very good performance, and is also abandoned. Therefore only two of the initial designs were selected for the final large-scale experiment on a Fenestron™ mock-up : #1 (classic SDOF) and #3 (SDOF+LEO).

TABLE 3 – Description of the 4 liner designs

Design	Type	Total thickness
#1	SDOF	26 mm
#2	DDOF (SDOF+SDOF)	31 mm
#3	DDOF (SDOF+LEO)	40 mm
#4	3xSDOF + 3xLEO	41 mm

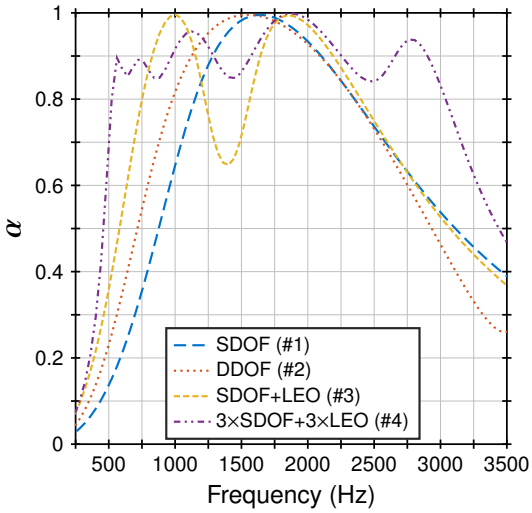

FIGURE 8 – Theoretical normal incidence absorption coefficients of the different designs, SPL=140 dB.

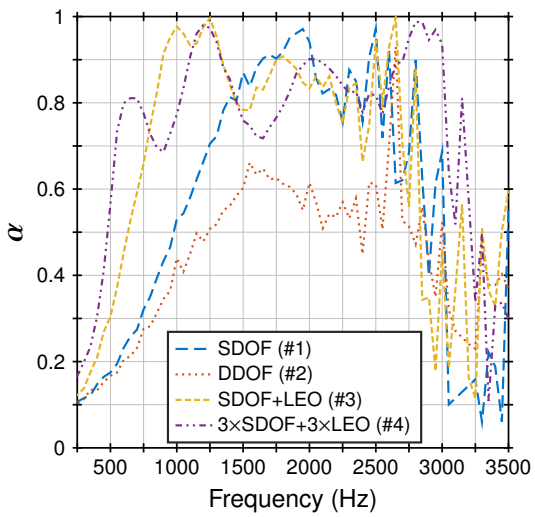

FIGURE 9 – Absorption coefficients of the different designs measured in the ONERA impedance tube, SPL=140 dB.

5. FENESTRON™ IN THE ANECHOIC ROOM

The following section focuses on the large-scale experimental campaign, where a Fenestron™ mock-up was equipped with liners to assess their efficiency in a realistic environment.

5.1 Description of the setup

The 1/3-scale mock-up used for this campaign is a test rig developed by Airbus Helicopters for various research investigations on Fenestron™ design, in which the rotor is driven by an electric motor and the blade pitch is controlled with an hydraulic system. The mock-up also includes multiple sensors allowing for measuring several state parameters. Rotor rotational speed and blade pitch can be controlled, thus enabling to perform tests at given thrust settings.

The mock-up is placed inside the anechoic room at ONERA (Fig. 10), suspended by a pole to the ceiling to keep the floor available for the placement of the acoustic antenna. The diffuser is oriented towards the open door, allowing airflow to exit the room. The mock-up is positioned as far from the walls as possible to ensure maximum airflow cleanliness, particularly around the collector.

The acoustic antenna is placed on the floor. It comprises 20 $^1/_4$-inch microphones and covers an area of roughly 4 m^2. It is positioned so that one microphone (#12 in Fig. 11) is aligned with the rotor's center, and the layout is symmetric around the rotor plane.

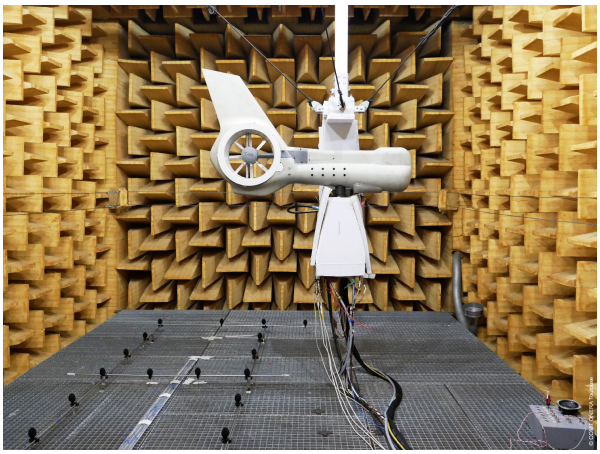

FIGURE 10 – Mock-up in the anechoic room

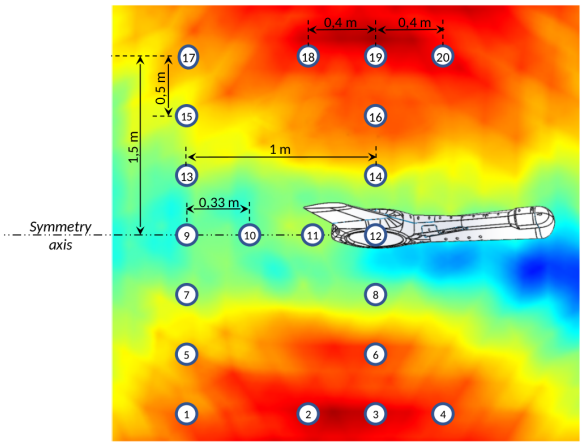

FIGURE 11 – Schematics of the acoustic antenna, superimposed to a simulated SPL field

5.2 Liner integration

The shroud of the 1/3-scale mock-up Fenestron™ is composed of three modular parts (Fig. 12):

- the diffuser (mainly pressure side) and the collector (mainly suction side), both allowing room for the integration of acoustic liners,
- the rotor plane where no acoustic liners was tested.

Three acoustic liner parts were manufactured :

- one of each design for the diffuser
- one with a geometry based on the SDOF design but adapted to the smaller internal space of the collector.

For simplicity during the test campaign, the DDOF (SDOF+LEO) liner design was renamed LEONAR. On the two diffuser parts, the acoustic liner covers roughly 80% of the available area due to the integration of drive shaft and supporting rods, while the collector

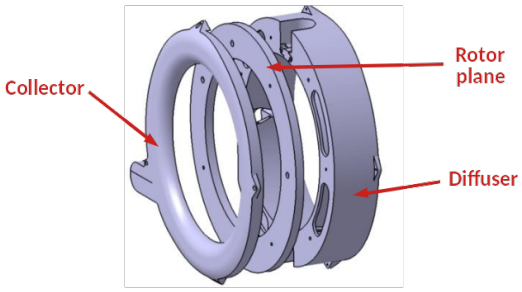

FIGURE 12 – Modularities

is perforated over its whole surface, including the lip. All parts, as well as the corresponding rigid parts, were manufactured using 3D-printing (see Fig. 13). Additionally, it was decided to perform tests on a configuration simulating a reduction of liners covering area by half for the LEONAR configuration, using added tape on the diffuser surface. This configuration is named ”LEONAR 50%” later in this paper.

5.3 Test matrix

The goal of the campaign was to test various configurations, to assess both the effect of the acoustic liners and the influence of aerodynamic interactions between diffuser and collector sides of the shroud. One configuration (#8) was also added to the experiment plan to investigate the effect of modifying the size of the fairing around the drive shaft on the generated noise (Fig. 14). The fairing named ”ST6” is a larger shaft fairing, with a front thickness of 35.6 mm (as seen by the airflow coming from the rotor), whereas ”ST1” corresponds to a no fairing configuration, i.e. transmission arm alone (25 mm front thickness). The ST6 fairing was used in all the acoustic configurations listed in Table 4. The following tables sum up the tested configurations.

TABLE 4 – Simplified test plan for the Fenestron™ campaign - Acoustic configurations (with reference ”Tripod+ST6” setup for the drive shaft system)

#	Diffuser	Collector	Rotor plane
1	Rigid	Rigid	Rigid
2	SDOF	Rigid	Rigid
3	LEONAR	Rigid	Rigid
4	SDOF	Perforated	Rigid
5	LEONAR (50%)	Rigid	Rigid
6	Rigid	Perforated	Rigid
7	LEONAR	Perforated	Rigid

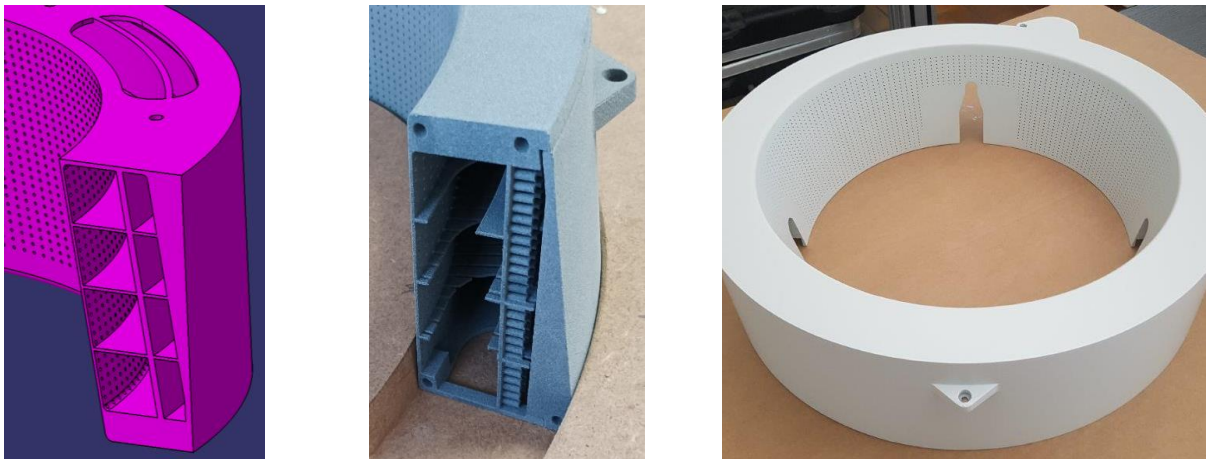

(a) CAD of the SDOF part (b) LEONAR part during assembly (c) Finished LEONAR part

FIGURE 13 – Manufacturing process for the diffuser parts

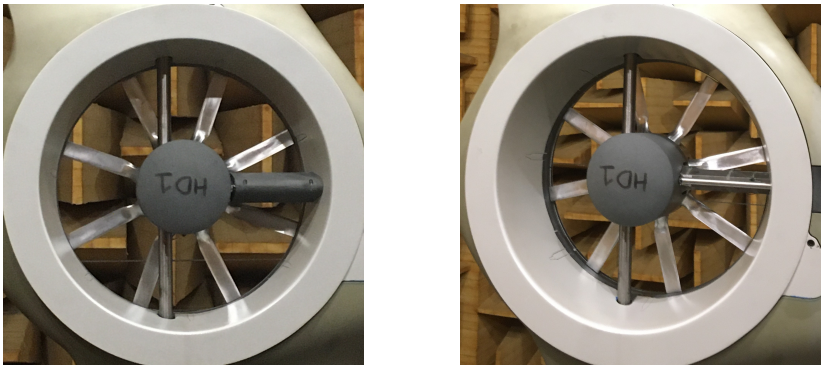

(a) Tripod ST6 (conventional fairing) (b) Tripod ST1 (no fairing)

FIGURE 14 – Different drive shaft fairings

TABLE 5 – Simplified test plan for the Fenestron™ campaign - Aerodynamic configurations, with the reference ”Rigid” setup (i.e. without any acoustic treatment)

#	Diffuser	Collector	Drive shaft fairing
1	Rigid	Rigid	Tripod + ST6
8	Rigid	Rigid	Tripod + ST1

6. RESULTS

6.1 Acoustic treatment of the shroud

This part focuses on results from the configurations listed in Table 4, to assess the effect of adding liners to the Fenestron™ duct.

6.1.1 Computation of the attenuation

For the acoustic analysis, the value of interest (focusing on tonal components which present the best signal-to-noise ratio) is the SPL in the narrow band corresponding to the 1st BPF for each configuration. This enables to assess the behavior of the acoustic treatments over a large range of frequencies, from lowest 1st BPF around 730 Hz to highest 1nd BPF around 1600 Hz.

For each frequency (1st BPF at a given RPM and pitch), the attenuation at a specific microphone is computed by comparing the obtained SPL to the reference value measured by the same microphone in the fully rigid case #1 :

$$\text{Attenuation}_{meas}(f) = \text{SPL}_{ref}(f) - \text{SPL}_{meas}(f) \quad (2)$$

where RPM and pitch are identical and f is the considered frequency.

The area covered by the antenna is divided into three zones (Fig. 15), each corresponding to a region where different acoustic phenomena are expected following the preliminary simulations (see Fig. 6) :

— zone 1 : collector
— zone 2 : under the duct
— zone 3 : diffuser

Within each zone, the sound pressure levels (SPL) from all microphones are averaged for each frequency selected in the analysis, effectively treating each zone as a single microphone. Combined with Equation 2, this approach thus yields three comparative values per configuration.

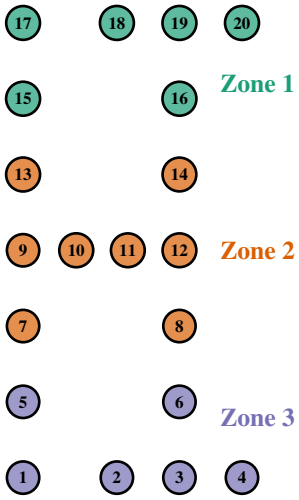

FIGURE 15 – Division of the antenna in 3 zones (the upstream zone is zone 1)

6.1.2 Acoustic treatment efficiency

Figure 16 shows the attenuation obtained in each zone for configurations with a treated diffuser at two different blade pitch angles.The maximum Fenestron™ pitch is more representative of high thrust flight conditions such as climb phase, while 0° Fenestron™ pitch is more appropriate for approach flight condition with limited generated thrust. The angle denoted θ_{max} is determined as the blade pitch angle that leads to an approximately ”constant” thrust when varying RPMs : the blade angle is thus different for each frequency plotted but thrust values are similar.

The effect of the acoustic liners are clear, especially in zones 2 and 3 (below and on diffuser side of the Fenestron™). At maximum pitch, the design including LEONAR cells is more effective than the classic SDOF one, especially at lower frequencies, with up to 7 dB more attenuation under the shroud ; this is partly due to its reduced sensitivity to aerodynamic effects. Moreover, the LEONAR design offers a more broadband absorption than the SDOF design in the same conditions. The influence of the total treated area is visible when comparing the attenuations obtained in configurations #3 and #5 at low frequencies : reducing the open perforated area reduces the maximum attenuation by several dBs in zones 2 and 3, while zone 1 is quite unaffected. Similar trends appear at neutral (0°) pitch, with some exceptions at higher frequencies that might be due to small variations in the pitch.

Figure 17 shows the same results for the configurations with the treated collector part, with the fully rigid configuration #1 still used as reference. The effect of the collector alone (#6) is quite low, except in zone 1 near the estimated resonant frequency of the cavity. When used in combination with a treated diffuser part (#4 and #7), the performance is similar for both treatments, and the attenuation is lower than with a treated diffuser alone in most cases : this might be due to a modification of the aerodynamic interactions around the shroud that is not fully understood yet. This phenomena was partly expected following the numerical simulations : as can be seen in Figure 6, the total SPL mitigation can be greater with the treated diffuser alone than with the treated collector and the treated diffuser together in some configurations. Thus, even if the model used for the preliminary numerical simulations does not take into account the air flow around the duct, the results obtained numerically give a quite correct tendency for the experimental results.

Figure 18 shows the same measurements focusing on a specific pair of RPM/pitch values representative of a helicopter climb situation, for several configurations of the Fenestron™ shroud. On average, the LEONAR and SDOF diffusers (respectively #3 and #2) offer similar noise mitigations, however the LEONAR treatment performs clearly better than the SDOF treatment for reducing noise under the flying path (zone 2). Combining a treated diffuser and collector (#4) does not seem to add much compared to having only a treated diffuser (#2) in this specific situation.

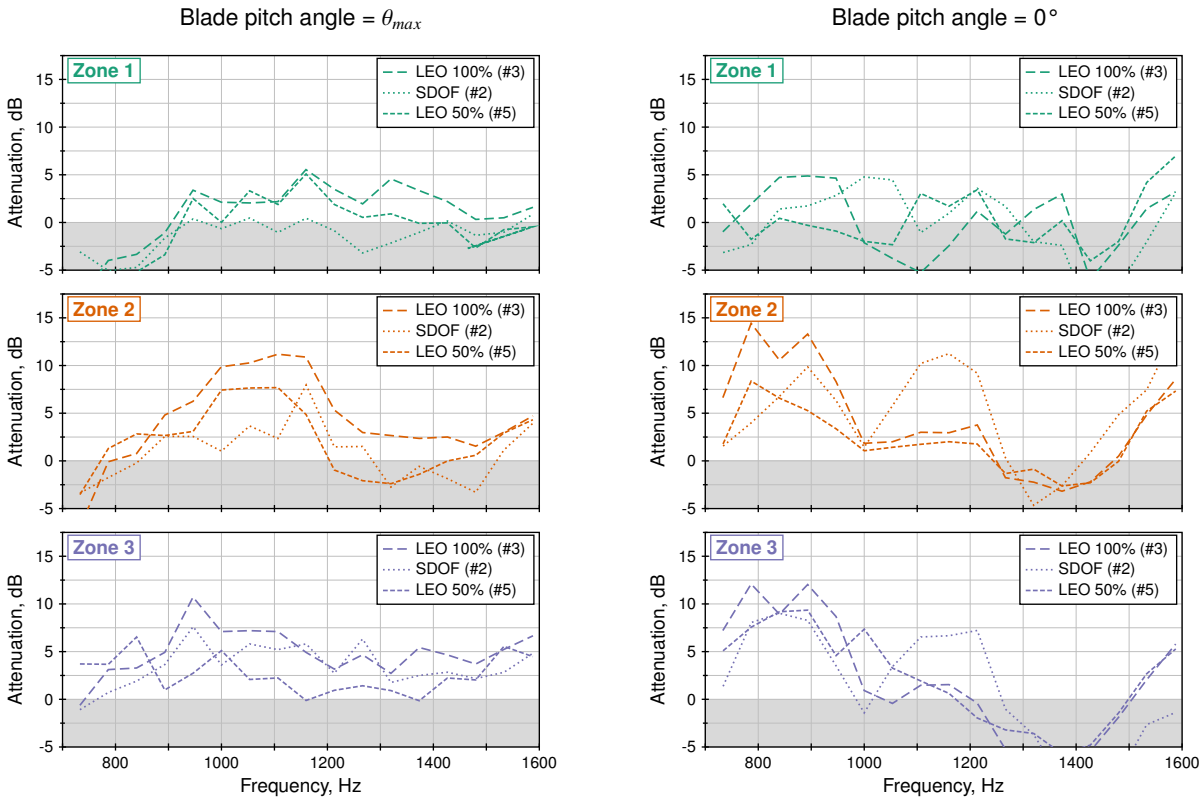

FIGURE 16 – Acoustic attenuation by zone : cases with treated diffuser

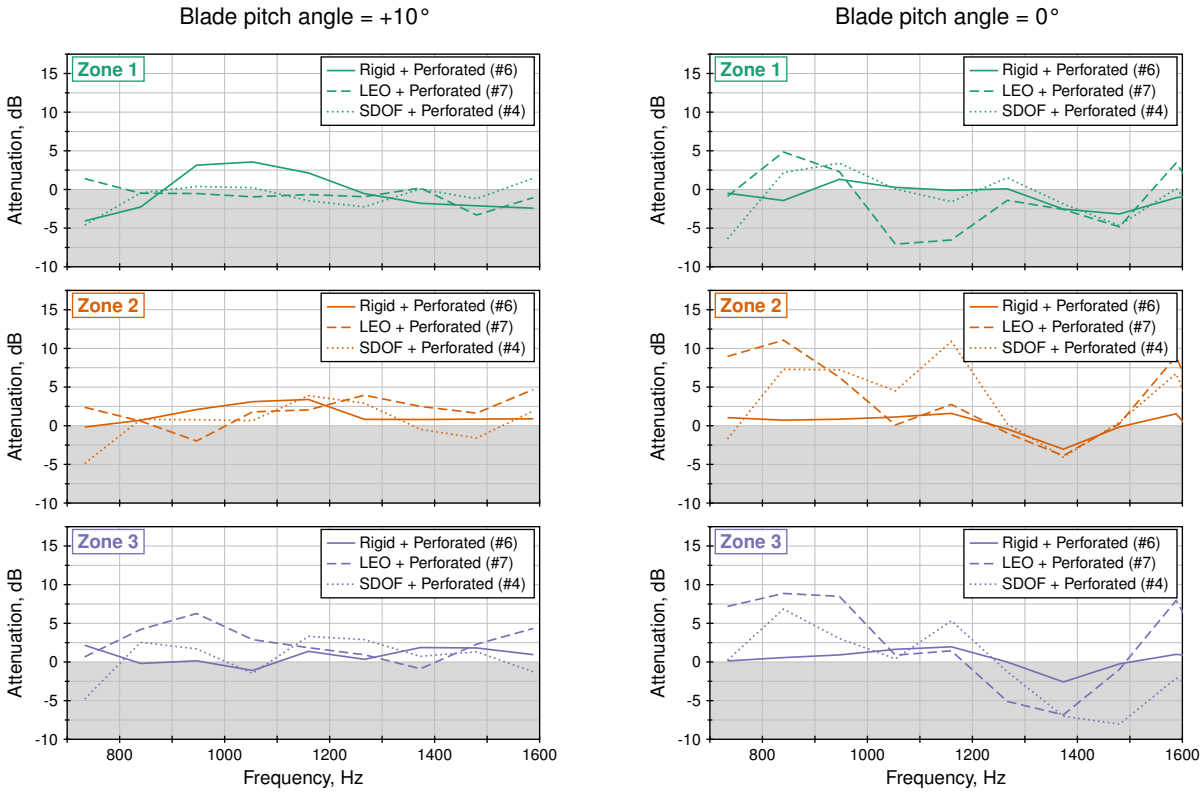

FIGURE 17 – Acoustic attenuation by zone : cases with treated collector

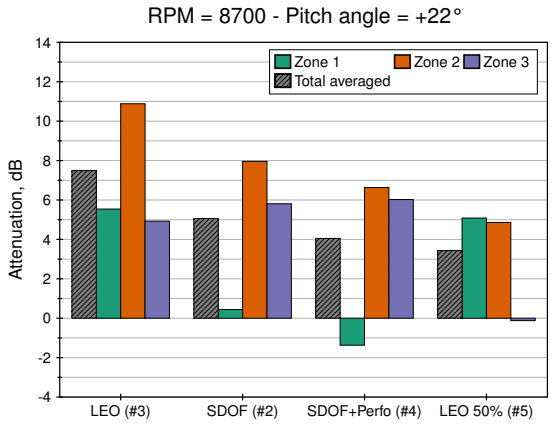

FIGURE 18 – Comparison of the obtained attenuation (total and by zone) for selected diffuser configurations, at a RPM/pitch representative of a take-off situation.

6.2 Acoustic effect of the drive shaft

The objective of these measurements was also to gather some insight on the aerodynamic interactions between the rotor and the transmission arm and assess the effect of modifying the drive shaft fairing in size.

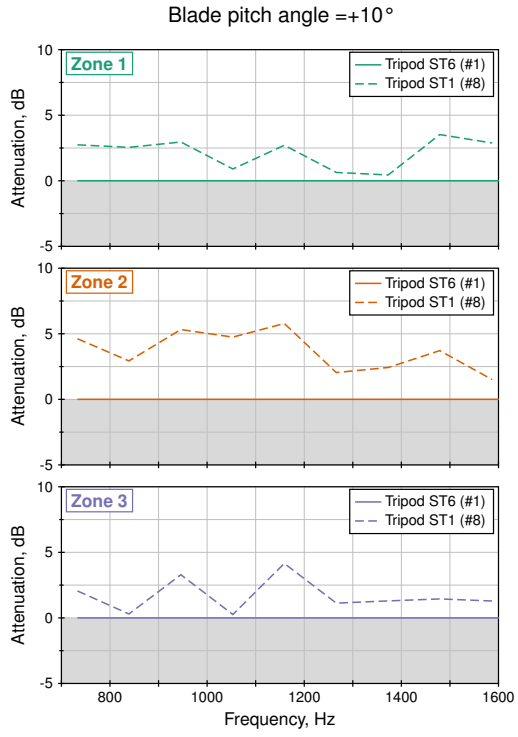

FIGURE 19 – Effect of different drive shaft fairings.

Results for the test cases presented in Table 5 are shown in Fig. 19. Once again, the attenuation correspond to the difference with the reference SPL in configuration #1 (flat solid line), for each microphone zone. The added value of reducing the shaft fairing size (Tripod ST1) appears clearly, as the emitted acoustic level in this configurations is several dB lower than the reference level over most of the considered frequency range. This phenomenon, which was expected, is likely due to the reduction of interaction noise within the Fenestron™ duct.

7. CONCLUSIONS

1. A preliminary numerical optimization step using COMSOL Multiphysics® and the OPAL software (developed at ONERA) allowed to propose several liner designs adapted to a Fenestron™ environment. An experimental campaign on small-scale benches and samples at ONERA proved the pertinence of the optimization process and led to selecting the two best designs, both in terms of acoustic performance and industrialization potential.

2. The two designs were integrated into a 1/3-scale Fenestron™ mock-up, in both the diffuser and collector parts of the shroud, for a large-scale measurement campaign in an anechoic room at ONERA. This campaign proved the effectiveness of the added acoustic treatment on the Fenestron™ shroud, especially for reducing noise radiation under the helicopter's fin.

3. At maximum Fenestron™ pitch, representative of the conditions during climb phase, the results highlighted the importance of innovative liner design approaches, since the LEONAR concept showed a greater overall performance when compared to a more classical SDOF solution.

4. This research allowed also to quantify the aeroacoustic effect of the drive shaft fairing design on noise emissions of the Fenestron™.

Perspectives of this study include an assessment of the benefits of these technologies on actual helicopter noise levels, leveraging on the methodology presented in [16].

Author contact :

Victor Lafont	victor.lafont@onera.fr
Delphine Sebbane	delphine.sebbane@onera.fr
Frank Simon	frank.simon@onera.fr
Julien Caillet	julien.caillet@airbus.com
Jean-Paul Pinacho	jean-paul.pinacho@airbus.com

8. ACKNOWLEDGMENTS

The authors warmly thank Laurent Burel and Nicolas Fasano from ONERA for their help in setting up all the experiments presented in this paper. In the same way, Laurent Jauffret, Christophe Lambert, Benoit Blondel and Vincent Girard from the Airbus Helicopters Laboratory Department are warmly thanked for their work on the Fenestron™ model design, installation and operation.

Rémi Roncen is gratefully acknowledged for his work on OPAL and his generous help during the preliminary phase of liner design.

This research has been carried out within the Airbus Helicopters - ONERA research program MOTUS, partly supported by the French Civil Aviation Authority through the French recovery plan and by the European Commission through NextGeneration UE.

9. REFERENCES

[1] R. Pongratz and D. Redmann, “Acoustic liner design for Fenestron® noise reduction,” 42nd European Rotorcraft Forum, Lille, France, 2016.

[2] S. Schneider, R. Heger, and P. Konstanzer, “Bluecopter™ demonstrator : The state-of-the-art in low noise design,” 42nd European Rotorcraft Forum, Lille, France, 2016.

[3] R. E. Motsinger and R. E. Kraft, “Design and performance of duct acoustic treatment,” *Aeroacoustics of Flight Vehicles : Theory and Practice. Volume 2 : Noise Control*, 1991.

[4] M. G. Jones, F. Simon, and R. Roncen, “Broadband and low-frequency acoustic liner investigations at NASA and ONERA,” *AIAA Journal*, vol. 0, pp. 1–20, Jan. 2022.

[5] Y. Murata, T. Ishii, S. Enomoto, H. Oinuma, K. Nagai, J. Oki, and H. Daiguji, “Experimental research on new acoustic liners combined with fine-perforated-film,” in *28th AIAA/CEAS Aeroacoustics 2022 Conference*, p. 2885, 2022.

[6] F. Simon, “Long Elastic Open Neck Acoustic Resonator for low frequency absorption,” *Journal of Sound and Vibration*, vol. 421, pp. 1–16, 2018.

[7] C. Yang, P. Zhang, S. Jacob, E. Trigell, and M. Åbom, “Investigation of extended-tube liners for control of low-frequency duct noise,” *AIAA Journal*, pp. 1–16, 2021.

[8] J. Guo, Y. Fang, Z. Jiang, and X. Zhang, “An investigation on noise attenuation by acoustic liner constructed by Helmholtz resonators with extended necks,” *The Journal of the Acoustical Society of America*, vol. 149, no. 1, pp. 70–81, 2021.

[9] F. Simon, R. Roncen, P. Vuillemin, P. Klotz, F. Méry, and E. Piot, “Design and optimization of acoustic liners with a shear grazing flow : OPAL software platform description,” in *INTER-NOISE and NOISE-CON Congress and Conference Proceedings*, vol. 263, pp. 508–518, Institute of Noise Control Engineering, 2021.

[10] R. Roncen, P. Vuillemin, P. Klotz, F. Simon, F. Méry, D. Sebbane, and E. Piot, “Design and optimization of acoustic liners with a shear grazing flow : OPAL software platform applications,” in *INTER-NOISE and NOISE-CON Congress and Conference Proceedings*, vol. 263, pp. 152–163, Institute of Noise Control Engineering, 2021.

[11] I. Garrick and C. E. Watkins, “A theoretical study of the effect of forward speed on the free-space sound-pressure field around propellers,” tech. rep., 1953.

[12] D. B. Hanson, “Helicoidal surface theory for harmonic noise of propellers in the far field,” *AIAA journal*, vol. 18, no. 10, pp. 1213–1220, 1980.

[13] D. B. Hanson, “Influence of propeller design parameters on far-field harmonic noise in forward flight,” *AIAA Journal*, vol. 18, no. 11, pp. 1313–1319, 1980.

[14] F. Simon, V. Lafont, D. Sebbane, J.-P. Pinacho, and J. Caillet, “Feasibility of an acoustic liner applied to a Fenestron : simulation,” in *INTERNOISE 2024*, 2024.

[15] V. Lafont, F. Simon, D. Sebbane, J.-P. Pinacho, and J. Caillet, “Feasibility of an acoustic liner applied to a Fenestron : experimentation,” in *INTERNOISE 2024*, 2024.

[16] F. Guntzer, J. Caillet, J.-P. Pinacho, P. Dieumegard, and E. Roca León, “A comprehensive helicopter acoustic modeling tool based on simulation and experiment,” 49th European Rotorcraft Forum, Bueckeburg, Germany, September 2023.